NJC

New Journal of Chemistry

An international journal of the chemical sciences

www.rsc.org/njc

Volume 33 | Number 3 | March 2009 | Pages 441–684

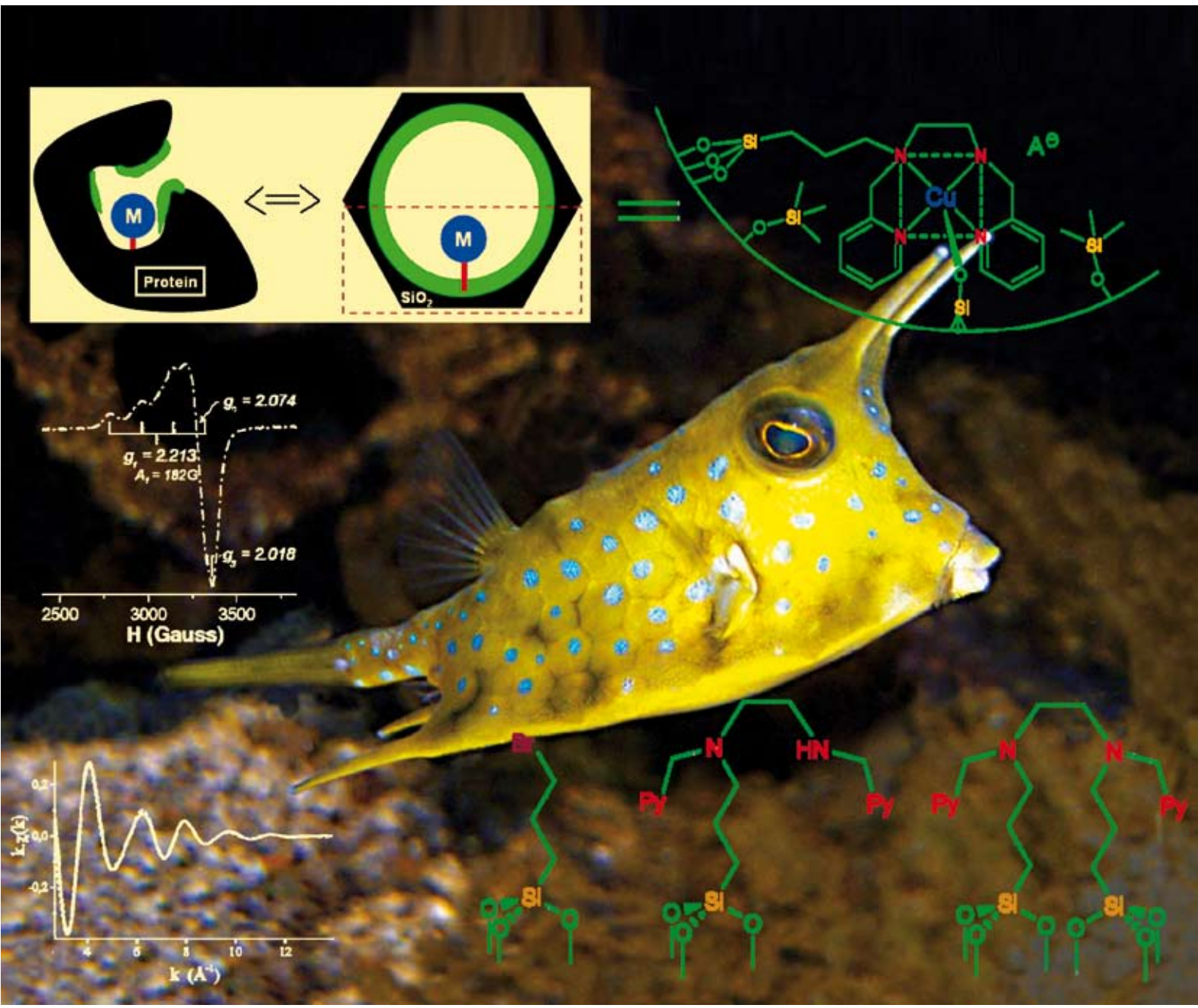

ISSN 1144-0546

RSC Publishing

PAPER
Laurent Bonneviot *et al.*
Design of grafted copper complex in mesoporous silica in defined coordination, hydrophobicity and confinement states

1144-0546(2009)33:3;1-0

Design of grafted copper complex in mesoporous silica in defined coordination, hydrophobicity and confinement states†

Sébastien Abry,[a] Aurore Thibon,[b] Belén Albela,[b] Pierre Delichère,[c] Fréderic Banse[b] and Laurent Bonneviot*[a]

Received (in Montpellier, France) 31st July 2008, Accepted 26th September 2008
First published as an Advance Article on the web 5th January 2009
DOI: 10.1039/b813031k

A bio-inspired synthesis of a silica grafted polydentate copper(II) complex is developed following the structural concept of metalloproteins where well defined metal ion coordination state, hydrophobic environment and confined space are present. Mesostructured porous silica of MCM-41 type replaces the proteic matrix while the pore surface is engineered according to a molecular stencil patterning technique combining both partial hydrophobization and site isolation in order to mimic the enzymatic cavity. The overall five-step synthesis includes the sol–gel formation of the silica matrix followed by partial removal of the structure directing agent and, sequential surface chemical modifications. This new methodology is illustrated here using trimethylsilyl functions to dilute bromopropylsilyl tripod tethers that undergo, directly in the pores, in a subsequent step nucleophilic substitution by a tetradentate ligand *N*,*N*′-bis(2-pyridinylmethyl)ethane-1,2-diamine (L_4^2). The metallation of the grafted ligand is obtained in the final step by merely contacting the solid with copper(II) chloride or triflate ethanolic solutions. Different techniques such as powder XRD, N_2 adsorption–desorption, elemental analysis, IR, XPS, EPR and EXAFS were combined together with an emphasis on quantification to reach a quasi-molecular description at each functionalisation step of the internal surface of the materials.

Introduction

Molecular transportation, vectorization, signalling, transformation, catalytic conversion, and many other functions are performed daily in living systems with an astonishing precision where diffusion control, regioselectivity, enantioselectivity are finely controlled to a level that conventional chemistry reaches only in rare cases and mostly through polluting processes. One of the most achieved living machineries at the heart of these complex and precise functions, are the proteins. They are supramolecular systems superficially resembling polymers with nonetheless a very precise environment at the molecular level that controls their folding. This morphology creates more or less hydrophobic open spaces where are nested functionalities, traditionally called enzymatic cavities for catalytic systems. Some of these use metals such as iron, copper, manganese or cobalt to carry out various functions such as oxygen transportation, selective oxidation with molecular oxygen, hydrogenation and C–C bond formation in presence of water and oxygen.[1] Trying to take their structure as conceptual models is an ongoing challenge currently taken up by a large community of chemists. Such a bio-inspiration is mostly devoted to mimic the coordination chemistry of the metal centre to better understand the molecular environment and the mechanism of action.[2] Few studies report on the combination of several sites (metal oligomers, Brønsted acid groups, phenoxy groups, *etc.*)[3,4] and rare are those combining coordination chemistry and confinement. Even fewer studies combine metal coordination control, confinement and hydrophobicity.[5,6] The present study reports on the design of such material where a bio-inspired *non-heme* complex is covalently retained in pores of calibrated size and hydrophobized internal surface.

The most common metal in metalloproteins is iron, which is most often engaged into *heme*-type‡ of complexes. However, an attractive feature of the *non-heme* ligands is the easiness of their chemical modifications for tuning catalytic properties in comparison with *heme*-type of ligands. Among them, pyridinylamino ligands have been used in the past years as relevant models for non-*heme* iron oxygenases.[7,8] In this line, Fe^{II} catalysts complexed by the tetradentate ligand L_4^2

[a] *Laboratoire de Chimie, Ecole Normale Supérieure de Lyon, Institut de Chimie de Lyon, Université de Lyon, 46 Allée d'Italie, 69364 Lyon Cedex 7, France. E-mail: laurent.bonneviot@ens-lyon.fr; Fax: +33 (0)4 72 72 88 60; Tel: +33 (0)4 72 72 83 91*
[b] *Institut de Chimie Moléculaire et des Matériaux d'Orsay, Laboratoire de Chimie Inorganique, Université Paris Sud 11, 91405 Orsay Cedex, France*
[c] *Institut de Recherches sur la Catalyse et l'Environnement de Lyon (UMR5256 CNRS), Université de Lyon, 2 avenue Albert Einstein, 69626 Villeurbanne, France*

† Electronic supplementary information (ESI) available: N_2 sorption isotherms at 77 K in Fig. S1, data from XPS analysis in Tables S1 and S2, and EXAFS fit quality criteria in Table S3. See DOI: 10.1039/b813031k

‡ Heme stands for a natural prosthetic group that consists of iron complexed by a conjugated heterocycle of porphyrin type; in biomimetic coordination chemistry conjugated heterocycles such as artificial phthalocyanines are considered by extension as heme-like while non-conjugated polydentate ligands are non-heme ligands.

(*N*,*N*′-dimethylbis(2-pyridinylmethyl)ethane-1,2-diamine) have shown interesting activity for alkane[9] and aromatic[10] hydroxylation using H_2O_2. A binuclear metal complex complexed by L_4^3 (N,N′-dimethylbis(2-pyridinylmethyl)propane-1,3-diamine), a ligand of the L_4^2 family, has also been found to be an efficient catalyst for alkane hydroxylation using O_2.[11] Though less important than iron, copper plays an important role in *non-heme* systems.[12] Analysing sequences in putative copper binding proteins (CBP) using advanced computational treatment on protein data base (PDB) reveals that copper binds preferentially through N-donor ligand (histidine, exclusively) and S-donor ligands (mostly cysteine and to a lesser extent methionine); the most representative coordination involving 2–6 side chains of the amino acids with three being the most common.[13] However, a CuN_4 environment is unlikely in CBP. Therefore, copper should be considered rather as a probe for L_4^2 in a preparatory work for designing iron catalysts than a model of a specific natural copper site.[14] This is also justified by a number of previous reports using UV-visible, EPR and EXAFS studies that are useful for characterizations.

A part of the metal centre, the proteic matrix molds the specific cavities where the sites are nested (Fig. 1). The protein self-folding is a very complicated process only emulated by oligopeptides that are too small to really recreate cavities. A pragmatic approach consists to reproduce some of the properties of the cavity such as the size in the nanometre scale of length and the hydrophobic character. According to this approach, some materials can conveniently be useful for that purpose. The best are those with calibrated sites of pores such as mesostructured mesoporous silica of MCM-41 type[15] or SBA type.[16] Though the long range periodicity of such materials is not necessary for catalytic applications, this is very useful for characterisation purposes in order to monitor the integrity of the inorganic matrix and the functionalisation efficiency during the various synthesis steps of the material.[17,18] In this context, our group has developed a multistep technique that allows to homogenously disperse two functions, F_1 and F_2, with molecular control of their vicinity.[19,20] This technique called *Molecular Stencil Patterning* (MSP) is based on the use of the surfactant acting as stencil covering the surface according to a regular pattern generated by electrostatic self-repulsion. The surfactant coverage level allows controlling the uncovered surface reacting during the grafting of F_1. Then, the surfactant molecules are removed in reaction conditions that retain F_1 on the surface. The grafting of the second function F_2 takes place at this step where the surfactant was located. Therefore, F_2 isolation is achieved for F_1/F_2 molar ratio higher than 2/3 assuming a full covered surface.[19,20] F_1 can be chosen to eventually control the hydrophobicity of the surface.

This study concerns the design of a material containing biomimetic copper sites (F_2) isolated by hydrophobic functions (F_1) according to MSP (Fig. 1 and 2). Such a multistep synthesis in the confined space of the nanochannels of the material is depicted by a retrosynthesis scheme given in Fig. 2. The copper(II) ions are retained in the channel of the LUS silica by metallation (step 5) of L_4^2 ligands, the fixation of which is obtained from the nucleophilic substitution of bromopropylsilyl tethers (step 4). The latter are grafted beforehand on the silica surface (step 3). The dispersion of

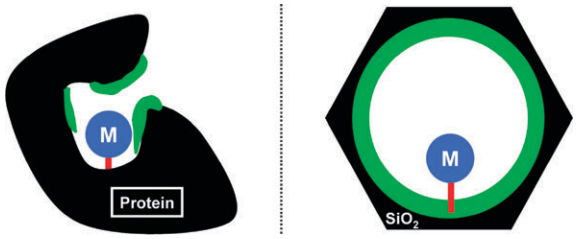

Fig. 1 Transposition from metalloprotein to mesoporous solid grafted metal complexes.

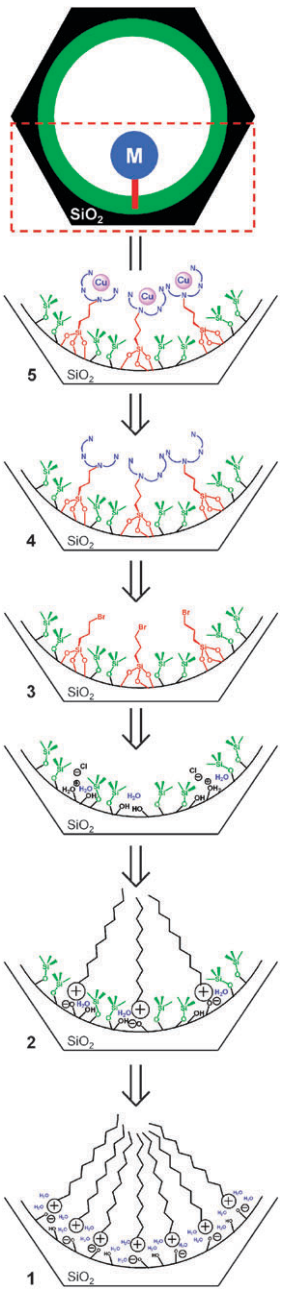

Fig. 2 Retrosynthetic route of material **5**.

the tethers is generated by the MSP technique comprising partial removal of the surfactant and silylation using hexamethyldisilazane (step 1) followed by extraction of the remaining surfactant (step 2). Each step produced a solid that was characterized structurally (XRD and porosity) and molecularly (XPS, EPR and EXAFS). Quantification has been pushed as far as possible combining elemental analysis, IR and XPS data.

Experimental

Materials

Hexadecyltrimethylammonium *p*-toluenesulfonate (CTATos) (>99% Merck), chlorotrimethylsilane (CTMS) (98% Acros), hexamethyldisilazane (HMDSA) (98% Acros), hexamethyldisiloxane (HMDSO) (98% Acros), Ludox HS-40 (40% SiO_2 Aldrich), (3-trimethoxysilylpropyl)diethylenetriamine (DETA) (95% ABCR-Roth) and 3-bromopropyltrichlorosilane (BPTCS) (97% ABCR-Roth) were used as received. Toluene, cyclohexane, acetonitrile were stored with molecular sieves under argon.

The ligand L_4^2 (*N*,*N*′-dimethylbis(2-pyridinylmethyl)-ethane-1,2-diamine) was synthesised following the method described by Goodwin and Lions.[21]

Preparation of materials

As-made silica 1[22,23]. The solid **1** was prepared as follows: Ludox (15.5 g, 0.26 mol) was added to sodium hydroxide (2 g, 5×10^{-2} mol) in deionized water (50 mL), then stirred at 313 K until clear (about 24 h). A second solution of hexadecyltrimethylammonium *p*-toluenesulfonate (CTATos) (2.5 g, 5.5×10^{-3} mol) in deionized water (90 mL) was stirred during 1 h at 333 K. The first solution was dropwise added to the second one, then stirred at 333 K during 2 h. The resulting sol–gel was heated in an autoclave at 403 K during 20 h. After filtration and washing with deionized water (approximately 300 mL), the as-synthesised solid **1** was dried at 353 K. Elemental analysis of **1**: C, 32.7; H, 6.7; N, 2.0, S, 0.4%; weight loss at 1273 K (49.3%). A BET specific surface area of 970 $m^2\ g^{-1}$ was obtained after solvent extraction (see below) and vacuum treatment at 423 K for 4 h.

Partially silylated silica 2. 5 g of **1** in technical ethanol (120 mL) were stirred at 313 K for a few minutes, then 5.1 mL (0.75 eq.) of hydrochloric acid (1 mol L^{-1} standard, Acros) were added. The mixture was stirred at 313 K for 1 h, then filtered, washed with technical ethanol (3 × 70 mL), technical acetone (2 × 50 mL), and dried at 353 K for one night, leading to 3 g of partially extracted silica.

The silica was then placed in a round bottom two-neck flask where it was dried at 423 K under argon flow during 1 h, then under vacuum during 2 h. On cooling back to room temperature, cyclohexane (100 mL) and hexamethyldisilazane HMDSA (20 mL) were added to the flask, the mixture was stirred at room temperature for 1 h, and refluxed for 17 h. The resulting mixture was filtered, washed with cyclohexane (3 × 70 mL), technical ethanol (3 × 70 mL), acetone (50 mL), and dried at 353 K for one h. These steps were repeated twice followed by an overnight drying at 353 K, leading to 3 g of partially silylated silica.

This solid was then treated with 1.1 equivalent of hydrochloric acid (1 mol L^{-1}) in technical ethanol (180 mL) at room temperature. The mixture was stirred for 1 h, then filtered, washed with technical ethanol (3 × 70 mL), acetone (2 × 50 mL), and dried at 353 K overnight, leading to 2.5 g of **2**. Elemental analysis of **2**: C, 5.9; H, 2.0; N, <0.10%; weight loss at 1273 K (11.5%).

Bromopropyl-functionalised silica 3. 2 g of **2** were placed in a round bottom two-neck flask and dried at 403 K during 1 h under nitrogen flow then 2 h under vacuum. Bromopropyltrichlorosilane (5 mL, 1.9×10^{-2} mol) was added under nitrogen flow in 50 mL of toluene containing the solid. The mixture was stirred at room temperature for 1 h, and then refluxed for 17 h.

The obtained product was washed with toluene (3 × 40 mL), technical ethanol (3 × 40 mL) and acetone (2 × 30 mL). The bifunctionalised silica was dried at 353 K leading to 2 g of **3**. Elemental analysis of **3**: C, 7.5; H, 2.1; N, <0.1, Br, 3.8%; weight loss at 1273 K (12.3%).

L_4^2-functionalised and capped silica 4. L_4^2 ligand (Scheme 1) (5 mmol) was dissolved in 10 mL of toluene. In parallel 2.1 g of **3** were placed in a round bottom two-neck flask where 10 mL of toluene was added. The L_4^2 solution was added to the flask containing the solid. The mixture was stirred at 308 K for 7 days. The obtained product was washed with toluene (3 × 30 mL), technical ethanol (3 × 30 mL) and acetonitrile (1 × 30 mL). The bifunctionalised silica was dried at 353 K overnight, leading to 2.3 g of solid.

This solid was then placed in a round bottom two-neck flask where it was dried at 353 K under argon flow during 1 h, then under vacuum during 2 h. On cooling to room temperature, cyclohexane (50 mL) and hexamethyldisilazane HMDSA (10 mL) were added to the flask, the mixture was stirred at room temperature for 1 h, and refluxed for 17 h. The resulting mixture was filtered, washed with cyclohexane (3 × 40 mL), technical ethanol (3 × 40 mL), acetone (30 mL). The bifunctionalised silica was dried at 353 K overnight, leading to 2.4 g of **4**. Elemental analysis of **4**: C, 14.0; H, 2.9; N, 1.4%; weight loss at 1273 K (15.1%).

Copper(II) supported complex 5a (Cl salt), 5b (OTf salt). 230 mg of solid **5** were placed in a round bottom flask with 10 mL of technical ethanol. A 3.4×10^{-2} mol L^{-1} solution of either $CuCl_2$ or $Cu(OTf)_2$ in ethanol was prepared. Then 4 mL of the copper solution were added to the solid suspension. The mixture was stirred at room temperature during 20 min, filtered and then washed three times with technical ethanol. The obtained silica was dried at room temperature for

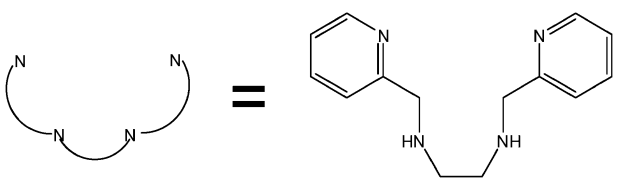

Scheme 1 Ligand L_4^2.

two days, leading to about 0,2 g of colored solid. The solid **5a** was obtained by metallation with copper(II) chloride and **5b** by metalation with copper(II) trifluoroacetate.

Elemental analysis of **5a**: C, 13.2; H, 2.9; N, 1.0; Cl, 1.8; Cu, 1.2; Si, 35.9% and **5b**: C, 12.7; H, 2.8; N, 1.0; S, 0.6; F, 1.3; Cu, 1.0; Si, 35.5%.

$[CuL_4^2]Cl_2$, 6a, and $[CuL_4^2](OTf)_2$, 6b. 56 mg of $CuCl_2 \cdot 2H_2O$ (0.33 mmol) or 119 mg (0.33 mmol) of $Cu(OTf)_2 \cdot 4H_2O$ were dissolved in 5 mL of technical ethanol. Then, 85 mg of L_4^2 (0.33 mmol) were added. A colored precipitate was immediately formed, which was filtered off, washed with ethanol and air dried, leading to **6a** (green) and **6b** (purple), respectively.

Methods used for characterization

XRD. Low-angle X-ray powder diffraction experiments were carried out using a Bruker (Siemens) D5005 diffractometer using Cu-Kα monochromatic radiation.

IR. Infrared spectra were recorded from KBr pellets using a Mattson 3000 IRTF spectrometer.

UV-Vis. Solution UV-visible spectra were recorded using a Vector 550 Bruker spectrometer. Solid diffuse reflectance UV-visible and near infrared spectra were recorded from aluminium cells with Suprasil 300 quartz windows, using a PerkinElmer Lambda 950 and PE Winlab software.

Nitrogen adsorption–desorption. Nitrogen adsorption–desorption isotherms at 77 K were determined with a volume device Micromeritics ASAP 2010 M.

TGA. TGA measurements (measure of weight loss at 1273 K) were collected from Al_2O_3 crucibles on a DTA-TG Netzsch STA 409 PC/PG instrument, under air (30 ml min^{-1}), with a 298–1273 K (10 K min^{-1}) temperature increase.

XPS. Surface experiments were performed in a KRATOS Axis Ultra DLD spectrometer equipped with a hemispherical analyzer, an axis magnetic lens and a delay line detector. The base pressure in the analysis chamber was better than 5×10^{-8} Pa. X-Ray photoelectron spectroscopy was performed using a monochromated Al-Kα X-ray source, with a pass energy of 10 eV and a coaxial charge neutraliser. Powder samples were pressed on indium foil, XPS spectra of Si 2p, N 1s, Br 3d, Cu 2p, Cl 2p, F 1s, O 1s and C 1s levels were measured at a normal angle with respect to the plane of the surface. High-resolution spectra were corrected for charging effects by assigning a value of 284.6 eV to the C 1s peak (adventitious carbon). Binding energies were determined with an accuracy of ±0.2 eV. Synthetic components on N 1s and Br 3d were analysed with a Shirley background subtraction and a peak shape with a combination of Gaussian and Lorentzian (30% Lorentzian).

EPR. EPR spectra were recorded using a Brucker Elexsys e500 X-band (9.4 GHz) spectrometer with a high sensitivity cavity at room temperature. The magnetic field was measured from a gaussmeter.

XAS. X-Ray absorption spectroscopy was performed at the European Synchrotron Facility (ESRF) in Grenoble (France) on the BM25 (Spanish) beamline at the Cu K edge (8979 eV). The EXAFS signals were extracted and simulated using the latest version of the EXAFS for Mac package including *RoundMidnight* simulation programs running on Mac OSX.[24] These standard EXAFS analyses[25] include a linear pre-edge background removal, polynomial and cubic spline atomic absorption calculation. MacMaster's table EXAFS spectra normalisation and reduction of the absorption data $\mu(E)$ to the EXAFS curve $\chi(k)$,[26] with k defined from E the photon energy and, E_0 the energy threshold (taken at half of the edge step at *ca* 8987 eV) were performed according to the following equation:

$$k = \sqrt{\frac{2m_e}{\hbar^2}(E - E_0)}$$

Pseudo-radial distributions $F(R)$ were calculated by Fourier transformations of the $k^3 w(k)\chi(k)$ in the k range 2.5–13.2 $Å^{-1}$; $w(k)$ is a Kaiser–Bessel apodisation window with a smoothness coefficient $\tau = 3.0$. The noise was removed by Fourier filtering. The fit was realized in the R range 107–280 pm (1.07–2.80 Å) that includes the first coordination sphere and the first next second neighbours, namely the carbon atom in α position in the amino ligand, L_4^2. It was shown in earlier reports that EXAFS multiple scattering pathways contribute mostly above 3.0, *i.e.*, out of the range of distances investigated here.[27,28] Therefore, the following single scattering EXAFS formula was sufficient to simulate the experimental data:

$$k\chi(k) = -S_0^2 \sum_i \frac{N_i}{R_i^2} [f_i(k, R_i)| e^{-2\sigma_i^2 k^2} e^{[-2R_i/\lambda(k)]} \times \sin[2kR_i + 2\delta_1(k) + \psi_i(k, R_i)]$$

where S_0^2 is the inelastic reduction factor, N_i is the number of equivalent scattering paths with an effective distance R_i, $\lambda(k)$ is the mean free path of the photoelectron, σ_i is the Debye–Waller coefficient due to distance distribution due to the atom vibrations (dynamic disorder) or due to site distribution (static disorder) for path *i*. $\delta_i(k)$ is the central-atom (or absorber) phase shift, and $f_i(k,R_i)$ and $\psi_i(k)$ are the amplitude and phase shift of the atomic scattering factors, respectively, calculated by the code FEFF on the structural models.[29] The use of theoretical phases and the uncertainty on the real position of the Fermi level, means the position of E_0 has to be adjusted during the fit. Therefore, there is a term ΔE_0 to adjust and for each set of atoms at a given distance (called a shell), there are three parameters to fit (R_i, σ_i and N_i). In the present case, assuming that all the nitrogen atoms can be grouped into a single shell with the same average distance, that there is only one second set of atoms due to the Jahn–Teller distortion in the Cu environment and the carbon in α position to the Cu-binding nitrogen, that leads to 10 parameters. A higher distortion or a mixture of species will rapidly impose more drastic simplification (*vide infra*).

The goodness of the fit is given by the minimum value of both statistical $\Delta\chi^2$ and reduced $\Delta\chi_v^2$ also named the quality factor, that depends on the number of independent points, N_{ind}, the total number of experimental points, N_{pt}, the experimental error ε_i^2, and the degree of freedom $\nu = N_{ind} - N_{par}$

for given number of parameters fitted in the simulation, N_{par} according to the following equation:

$$\Delta\chi^2_{stat} = \frac{N_{ind}}{N_{pt}} \sum_i \frac{[k\chi_{th}(i) - k\chi_{exp}(i)]^2}{\varepsilon_i^2}$$

$$\Delta\chi^2_{\nu} = \frac{\Delta\chi^2_{stat}}{\nu}$$

The accuracy of the simulation to reproduce the experimental data is estimated according to a standard statistical treatment procedure implemented in the program EXAFS for Mac.[24] The experimental noise is calculated according to the method proposed by Vlaic,[30] using the high frequency contribution of the EXAFS signal taken above 5.2 Å on the FT signal and the back-Fourier transformation.

Results

Synthesis

The ligand L_4^2 (Scheme 1) has been supported in a mesostructured porous silica considering the retrosynthetic scheme described in Fig. 2. The grafting of this polypyridinylamino ligand *via* a bromopropyl tether was performed on a partially hydrophobated mesostructured porous silica.

A LUS mesoporous silica possessing a 2D hexagonal structure was used as support.[17,22,23] The internal surface of the silica was then partially hydrophobated with trimethylsilyl (TMS) groups using the so-called molecular stencil patterning (MSP) approach developed by some of us.[17,19,31] This technique is designed to reach at full overall coverage an homogenous distribution of the TMS functions among the partially retained surfactant molecules acting as a mask. The latter are regularly distributed thanks to electrostatic self-repulsion. The removal of the remaining surfactant liberates the silanol functions available for further functionalisation.[20] This minimizes the inherent inhomogeneities occurring during direct grafting.[32] Then, a second function can be introduced, here bromopropylsilane (BPS) chosen as tether for the fixation of the L_4^2 amino ligand. The substitution reaction of the bromopropyl-functionalised silica **3** with the L_4^2 ligand was followed in soft conditions (35 °C, 1 week) in order to minimize leaching of the TMS groups. However, since a partial TMS loss was observed during the incorporation of related polypyridinylamino ligands in mesostructured materials,[20,33] a capping step using hexamethyldisilazane was required to achieve a maximal coverage of the internal surface (*vide infra*). Indeed, a full coverage of the surface was required to hinder the formation of copper silicate.[34] Two different salts of copper(II) were used to introduce the metal ion: copper chloride, $CuCl_2$, and copper trifluoromethanesulfonate, $Cu(OTf)_2$, in order to test the effect of the counter ion in the final material. Two materials possessing copper(II) complexes were finally obtained: **5a** (Cl) and **5b** (OTf).

Textural characterisation

The materials at each step of the synthesis were characterised by X-ray diffraction to check the integrity of the mesoporous structure. Diffraction patterns of materials **1**, **3**, **4** and **5a** (Fig. 3) reveal that the hexagonal structure of the solid is maintained through all the sequence of the synthesis, from the as-made LUS, **1**, to the supported copper complex in **5a**.

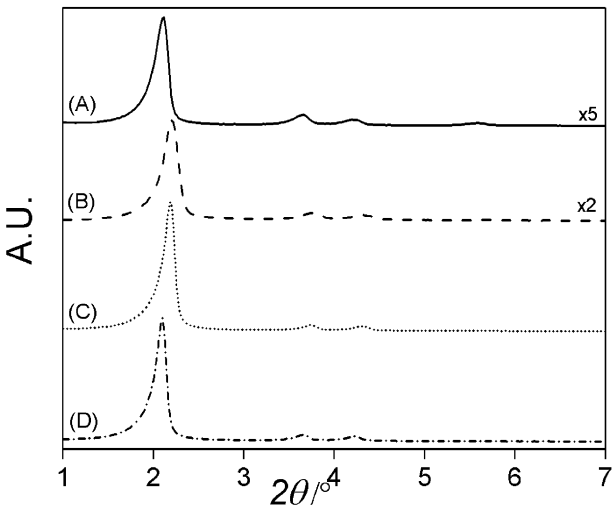

Fig. 3 Small angle powder X-ray diffraction of compounds: **1** (A), **3** (B), **4** (C) and **5a** (D).

The nitrogen sorption isotherms at 77 K of materials **1**, **2**, **3** and **5a** (Fig. S1, ESI†) are of type (IV) according to the IUPAC classification[35] and are characteristic of mesostructured porous materials.[36–38] The obtained profiles account for a narrow pore size distribution and a small average size pore diameter, decreasing from 3.7 nm in the LUS silica **1** to 3.3 nm in the final material possessing the copper complex, **5a**, according to the BdB model (Table 1). The specific BET surface area of the initial silica support **1** of 970 $m^2\ g^{-1}$ is gradually reduced during the synthesis sequence. Indeed, the partially silylated material possessing TMS groups presents a specific surface of 930 $m^2\ g^{-1}$, which is reduced upon successive incorporation of the bromopropyl tether and the L_4^2 copper complex to 750 and 590 $m^2\ g^{-1}$, respectively (Table 1). Concomitantly, the pore volume is gradually reduced from 0.86 $cm^3\ g^{-1}$ in the silica support **1** to 0.45 $cm^3\ g^{-1}$ in the final material **5a**. These results confirm the incorporation of the copper complex inside the pore of the mesostructured silica, while leaving enough place for the incorporation of other molecules such as a substrate for further catalytic applications.

Table 1 Textural analysis: BET specific surface area, A_{BET}, total pore volume, V_p, and pore diameter using the BdB method, ϕ_{BdB}

Samples	**1**	**2**	**3**	**5a**[d]
A_{BET}[a]/$m^2\ g^{-1}$	970	930	750	590
V_p[b]/$cm^3\ g^{-1}$	0.86	0.78	0.59	0.45
ϕ_{BdB}[c]/nm	3.7	3.4	3.4	3.3

[a] Measured in the P/P_0 range 0.1–0.25. Uncertainty: ±50 $m^2\ g^{-1}$. [b] Measured at $P/P_0 = 0.92$. Uncertainty: ±0.02 $cm^3\ g^{-1}$. [c] Using BJH calculation instead of BdB, the diameter would be 0.7 nm smaller in each case. Uncertainty: ±0.1 nm. [d] The textural characteristics for **5b** are within the accuracy the same as for **5a**.

Table 2 Quantification of grafted species reported in molar ratio otherwise stated from elemental analysis, TGA experiments (for weight loss at 1000 °C) and from quantitative IR spectroscopy.

Samples[a]	2	3	4	5a	5b
TMS/Si_{inorg}	0.12 ± 0.01 (~51%)[b]	0.13 ± 0.01 (~54%)[b]			
BPS/Si_{inorg}		0.038 ± 0.002 (~16%)[b]			
TMS + BPS[c]/Si_{inorg}			0.22 ± 0.02 (~91%)[b]	0.26 ± 0.03 (~108%)[b]	0.24 ± 0.02 (~101%)[b]
L_4^2/Si_{inorg}			0.021 ± 0.02 (~9%)[b]	0.019 ± 0.02 (~8%)[b]	0.018 ± 0.02 (~8%)[b]
L_4^2/mmol g^{-1}			0.24 ± 0.01	0.19 ± 0.01	0.18 ± 0.01
L_4^2/Cu				1.0 ± 0.1	1.1 ± 0.1

[a] TMS: trimethylsilyl, BPS: bromopropylsilyl, L_4^2: *N*,*N*′-bis((pyridin-2-yl)methyl)ethane-1,2-diamine ligand, Si_{inorg}: inorganic silicon from the silica wall (see text). [b] In parenthesis, coverage percentage of surface assuming 0.24 function/Si_{inorg} for full coverage (see text and refs. 17 and 19). [c] The presence of the ligand precludes any independent TMS quantification by IR spectroscopy.

Characterisation of the organic modifications

The different steps of the organic modification of the internal surface of the silica support **1** to obtain the final material **5a/b** were followed using a panel of techniques cited above. The quantity of grafted functions are gathered Table 2 with all values given in molar ratio relative to the inorganic silicon, Si_{inorg}. The latter, which is part of the mesostructured silica since there is no apparent structural modification, appears to be the best reference for a better molecular monitoring of the stepwise surface functionalisation.[17,19] Note also that the surface coverage is reported in percentages (parenthesis in Table 2) referring to a full molecular coverage of 0.24 mol/molSi_{inorg} whatever the nature of the grafted function. This is the maximum TMS coverage that can be obtained by reacting trimethylchlorosilane directly on the as-made LUS silica.[17,19] This value is also very close to 0.23 TMS/Si_{inorg} measured in a similar MCM-41 material.[31] The quantification of the TMS functions was also performed independently (in material **3**) using IR spectroscopy by integration of the peak at 845 cm^{-1} which corresponds to the Si–C stretching vibrations of the O–Si–$(CH_3)_3$ entities.[17]

In the first step, a partial silylation of the surface was performed, obtaining 0.12 TMS functions per mol of inorganic silicon. This value corresponds to *ca.* 50% of surface coverage. In the second step, 0.038 mol of bromopropyl tether were incorporated per Si_{inorg}, and no displacement of the TMS functions was observed (material **3**, Table 2). The overall coverage (TMS + BPS) is therefore 0.17 ± 0.01 functions/Si_{inorg}, *i.e.*, about 70%.

In material **4** after ligand fixation and capping, the amount of grafted functions is 0.22 function/Si_{inorg}, which indicates that 0.05 more TMS/Si_{inorg} have been added to the surface, leading to an overall coverage of 92%. This is obtained assuming no bromopropylsilyl removal during the amine (L_4^2) substitution for bromine, a reasonable hypothesis according to current studies on selective function degrafting.[39] This figure indicates that the capping treatment following the substitution reaction leads to a fully covered surface. The presence of L_4^2 ligand that exhibits some IR bands overlapping the band at 845 cm^{-1}, prevents independent quantitative IR study of TMS for this material. Fortunately, the L_4^2 content was estimated independently from N elemental analysis assuming that there was no other nitrogen source in material **4**. Indeed, according to the absence of –CH_2– stretching bands in the 2800–3000 cm^{-1} IR region, there is no ammonium surfactant in the solid **3** (before introduction of the ligand). The L_4^2/Si_{inorg} ratio is therefore 0.021 from elemental analysis (Table 2). In addition, from XPS (Table S1, ESI†), the N/Si_{total} atom ratio is 0.079 ± 0.004, which along with the correction from total to inorganic silicon, 0.023 L_4^2/Si_{inorg}. These data shows that both types of analysis lead to the same ligand loading within 10%.

The number of L_4^2 grafted corresponds to half of the bromopropyl tethers present in step 3, *i.e.*, before substitution. This could indicate that both amino groups of the L_4^2 ligand are implied in the substitution process leading to double tethered L_4^2 species (Scheme 2). However, the analyses reveal the presence of halogen remaining in the solid that could come (i) from chloride incompletely removed after the surfactant extraction treatment, (ii) from bromide resulting from the substitution reaction and, (iii) eventually from unreacted bromopropyl tethers. Since elemental analysis is inaccurate when a mixture of halogen is at stake, XPS was exploited preferentially allowing both independent element analysis and chemical state discrimination for bromine.

According to XPS, the overall Br/Si_{inorg} ratio is 0.012 (Table S1, ESI†), distributed in two XPS features arising at 68.2 and 70.6 eV assigned to negatively bromide ions (0.004 Br/Si_{inorg}) and neutral bromopropyl tethers (0.008 Br/Si_{inorg}), respectively (Table 3). These Br^- ions are likely retained in the pores by partially protonated amino groups of the grafted ligands.

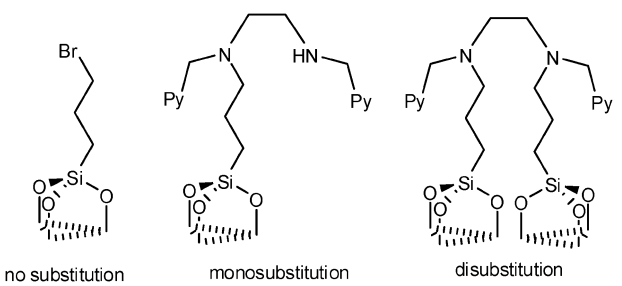

Scheme 2 Possible species on the surface of material **4**.

Table 3 XPS data for grafted ligand L_4^2 (material **4**) and grafted copper complexes (**5a** and **5b**). See Table S2 for binding energy in eV.

Sample		4	5a	5b
Br 3d/eV	% Br^-	32	26	24
	% Br	68	74	76
N 1s/eV	% N	86	91	91
	% N^+	14	9	9

The N 1s XPS spectrum of solid **4** is indeed consistent with this hypothesis. Two peaks at 399.3 (86%) and 401.7 (14%) (Table 3, Fig. 4(b) and Table S2, ESI†) are assigned to non-charged and positively charged nitrogen atoms of the L_4^2 amino ligand, respectively.[40] In fact, literature data suggest that the more intense peak is likely the superimposition of two features expected at 398.4 eV for the sp^3 neutral atoms of amine and at 400.0 eV for sp^2 N neutral atoms of pyridine.[41] The resolution is not good enough to simulate both contributions separately. It remains that the binding energy of 401.7 eV matches well with positively charged N atoms of ammonium ions, accounting for 0.013 ammonium per inorganic silicon (Tables 2, 3 and S2, ESI†). If one assumes one proton per L_4^2 moiety (a second protonation is unfavourable), this implies that *ca* 57% of the grafted ligands are monoprotonated.

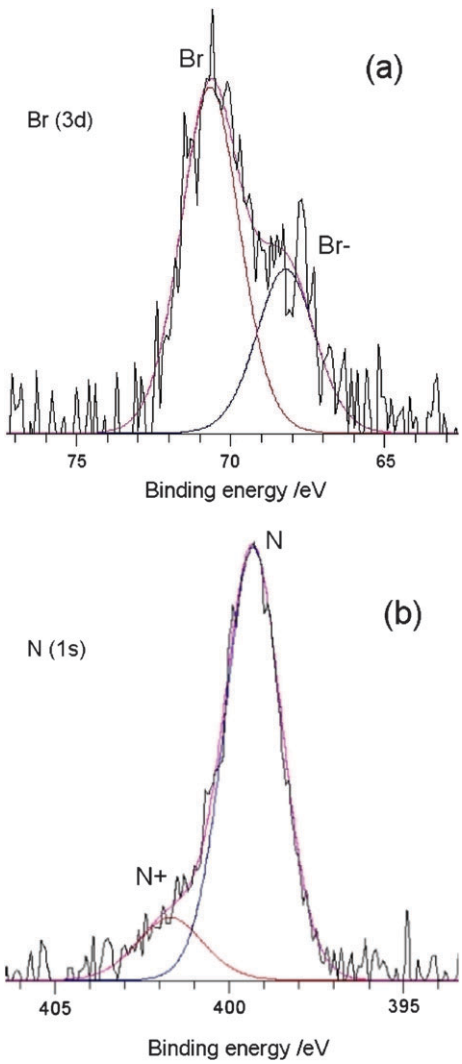

Fig. 4 XPS spectra of material **4**; (a) Br 3d and (b) N 1s: both with two deconvoluted curves (70% gaussian, 30% lorentzian; intensities given in Table 3).

The ligand metallation by copper salts does not change much the binding energy of either the Br 3d and N 1s peaks (Table S2,† materials **5a** and **5b**). However, the relative intensity of the peaks changes slightly consistently with a decrease of both charged Br and N atoms from *ca* 32 to 25% and 14 to 9%, respectively (Table 3). This is an indication that the complexation of the L_4^2 ligands by Cu(II) leads to a partial displacement of the proton and the bromide ions with still *ca* 37% of the ligand still monoprotonated (*vide infra*).

Characterisation of the metal center

The reaction of material **4** with $CuCl_2$ and $Cu(OTf)_2$ led to materials **5a** and **5b**, respectively, without significant carbon and nitrogen balance change according to elemental analysis. This indicates that there is no significant displacement of TMS or grafted ligands during this treatment (Table 2). By contrast, XPS analysis reveals that there could be a loss of ligand at the surface of the mesoporous particles. Indeed, there is a decrease of the N/Si_{total} atom ratio (Table S1, ESI†), which is moderate in material **5a** (*ca* 15%) and more pronounced in material **5b** (*ca* 33%). Material **5a** shows also a better consistency between elemental and XPS analyses than material **5b** regarding the copper loading (0.019 and 0.018 Cu/Si_{inorg} for the former and 0.016 and 0.008 Cu/Si_{inorg} for the latter, respectively). This shows again that the surface has undergone less damage and less copper loss in **5a** than in **5b**. The ligand to copper molar ratio of 1.0 and 1.1, respectively, is consistent with a nearly total complexation yield. The counter ion to copper ratio of 1.3 (chloride) and 1.1 (triflate, analyzed from F and S), respectively, indicates that copper neutrality is half accounted for by the material itself, most likely, silanolate groups.

A comparative spectroscopic study of materials **5a** and **5b** with the corresponding molecular complexes, **6a** and **6b** has been performed. The diffuse reflectance spectra are characterized by a strong band the maximum of which increases from 578 to 786 nm, from compounds **6b** to compounds **6a**,

Table 4 Spectroscopic data from DR UV-visible and EPR

Sample	6a	5a	5b	6b
λ^a/nm	786	740	668	578
g_1	2.261	2.228	2.213	2.219
g_2	2.083	2.094	2.074	2.058
g_3	2.019	2.036	2.018	1.994
$g_{iso}{}^b$	2.121	2.119	2.102	2.090
A_1/G	160	157	182	183
δ^c	0.36	0.43	0.40	0.40

UV-Vis spectra were recorded in solid state for all the samples. EPR spectra were recorded in the solid state at room temperature for materials **5a** and **5b**, and in MeOH solution at 150 K for the molecular complexes **6a** and **6b**. [a] λ corresponds to the maximum of the absorption peak observed in the DR UV-visible spectrum, ($\pm$1 nm). (g_1, g_2, g_3) parameters and the hyperfine coupling constant A_1 values have been deduced from the EPR spectra as shown in Fig. 5. Accuracy for g_i is $\pm$0.002 and for $A_1 \pm 2$ G. [b] g_{iso} is calculated from $g_{iso} = 1/3(g_1 + g_2 + g_3)$. [c] Orthorhombicity factor δ is defined as $\delta = (g_2 - g_3)/(g_1 - g_2)$.

respectively (Table 4). The spectra of materials **5a** and **5b** exhibit intermediate positions at 740 and 668 nm, respectively. Compared to the wavelength expected for copper directly adsorbed on silica (735 nm),[42,43] the value observed for material **5b** is a strong indication that copper is complexed by the grafted L_4^2 ligand. However, for material **5a** no conclusion can be drawn from this technique only.

The EPR spectra of the molecular complexes **6a** and **6b** exhibit a rather isotropic signal in EtOH solution at room temperature. Below the freezing temperature of EtOH leading to molecular rotation blockage, the signal becomes rhombic with the g tensors and A_1 (Cu) reported in Table 4. By contrast, for materials **5a** and **5b**, the signal is already rhombic at room temperature and exhibits the same features at 150 K (no linewidth, nor shape changes, see Fig. 5). This is consistent with rotation blockage in the materials as observed for direct adsorption of copper on silica when covalent interaction with the surface is present.[44,45] The absence of any isotropic signal also evidences the absence of any physisorbed ligand complexed to copper.

The g values reported in Table 4 ($g_1 \sim 2.22$, $g_2 \sim 2.08$, $g_3 \sim 2.03$) are consistent with a distorted copper(II) ion environment in materials **5a** and **5b**. A closer examination reveals a roughly axial situation where g_1 value can be assimilated to $g_{||}$, while g_2 and g_3, close one to another, would be related to the equatorial plane. In both materials, $g_{||} < g_2 \approx g_3 > 2.0023$, which reveals that $d_{x^2-y^2}$ is the magnetic orbital and is consistent with an elongated square pyramidal or elongated octahedral environment for Cu(II).[46,47] The rhombic distortion may be quantified by the factor $\delta = (g_2 - g_3)/(g_1 - g_2)$ equal to ~ 0.40 according to Hathaway *et al.*[48] These distortions are in agreement with the presence of a Jahn–Teller distortion typical for d^9 ions. In addition, the spectra of materials **5a** and **5b** show three of the four hyperfine lines arising from the hyperfine (HF) coupling of the unpaired electron with Cu nucleus (^{63,65}Cu, $I = 3/2$). These four lines centred on g_1 allow to determine the HF coupling constant A_1 ($= A_{||}$) to be 163×10^{-4} cm^{-1} (157 G) and 189×10^{-4} cm^{-1} (182 G) for **5a** and **5b**, respectively.

It appears as general trend from the g tensor that copper(II) is in a similar environment in materials **5a** and **5b**. The largest differences are observed for the molecular compounds **6a** and **6b**. One notes that the same trend is observed for the absorption maxima of the electronic transition in the visible region. Such an evolution is clearly related to ligands other than L_4^2 lying in the first coordination sphere of copper. These are eventually, triflate ions, chloride ions, water molecules or remaining surface silanolate groups. The presence of such type of ligands, usually called exogenous ligands in metalloproteins, will be investigated with the help of EXAFS data and discussed in the following.

The k weighted EXAFS signals are typically comprised of six oscillations the first three being much more intense than the others revealing some interferences that will appear clearly in the simulations. This fast damping precludes any studies above 13.5 Å^{-1} (Fig. 6). This situation is in all the cases due to a rather distorted environment, for the molecular models, $CuL_4^2Cl_2$ (**6a**) and $CuL_4^2(OTf)_2$ (**6b**) and for the grafted complexes in agreement with the EPR data. The FT

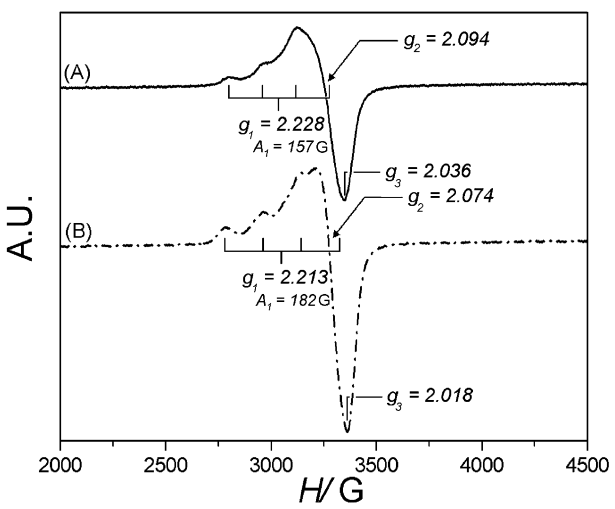

Fig. 5 X-Band EPR spectra at 298 K of mesostructured LUS silica after metallation by either copper(II) chloride (**5a**) (A) or copper(II) triflate (**5b**) (B). EPR spectra were recorded at room temperature with the following parameters: frequency: 9.35 GHz, power: 6.37 mW, modulation amplitude: 1 G, modulation frequency: 100 kHz.

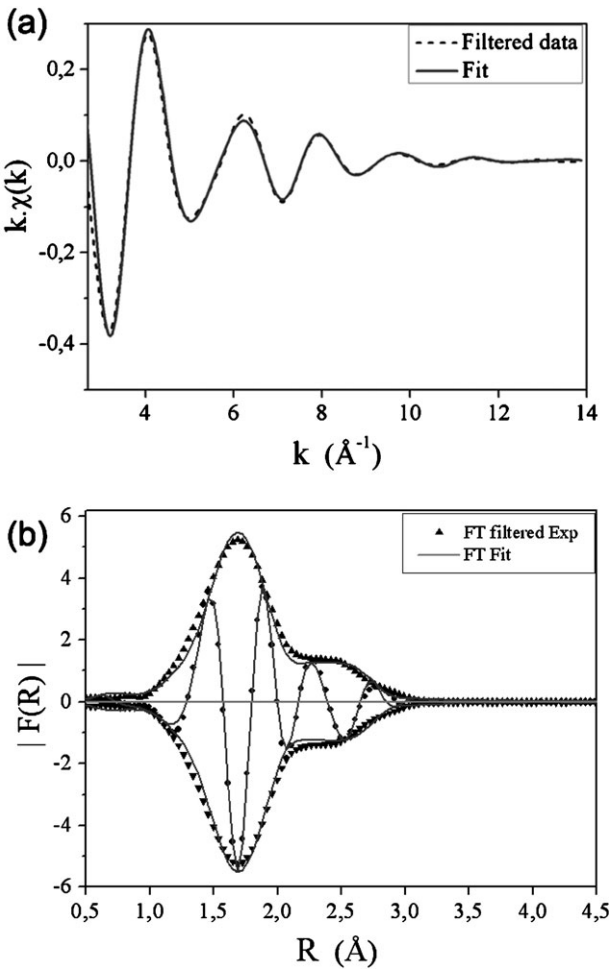

Fig. 6 EXAFS signal of material **5a**: (a) experimental oscillations filtered between 107 and 283 pm and simulated signal, and (b) their Fourier transforms.

transforms are characterized by two main peaks in the *R* interval 107–290 pm. The first one is assigned to the first coordination sphere that accounts for neighbours arising between 200 and 240 pm (2.00 and 2.40 Å) from the copper metal center. Note here that the FT signal is not phase corrected leading to FT peaks shifted by *ca* −40 pm for N, O or C backscattering atoms. The second FT peak appears as a shoulder of the first peak. FT filtering does not allow to separate both peaks for independent fitting. This situation reveals the presence of absorber atoms in an intermediate range of 240–290 pm where are expected the oxygen ligands. The third range of distances 280 to 320 pm corresponds to carbon atoms in α position of the amino and the pyridinyl groups of the L_4^2 ligand. The latter are indeed simulated without the need of multiple scattering theory at about 285 pm as expected for this kind of complexes[28,49] and are contributing mostly to the second FT peak centred at 250 pm (Fig. 6(b)).

In fact, the EXAFS simulation has to be treated at once with all the backscattering atoms because of the strong interference interplay between the different contributions. It is worth mentioning that the presence of destructive interferences precludes any precise determination of coordination number but allows very good distance determination as reported on Table 5. In addition, the restricted *k* and *R* ranges of the spectra impose a limited number of parameters. For materials **5a** and **5b**, only eight and seven parameters could be varied while the coordination number could not be fitted otherwise, the degree of freedom of the calculation would have been too small to reach a decent fit (QF would have been larger than unity). Therefore, simulations were performed using different models with no refinement of the coordination numbers: environments with 4 N (or O) close neighbours at about 200 pm and farther neighbours at 220–280 pm that are any combinations of 1 or 2 O or Cl atoms. Trials were also attempted with equivalent environments with only three instead of four close neighbours.

Table 5 Simulation parameters of the Cu K-edge EXAFS for model complexes, **6a** and **6b**, and materials **5a** and **5b**

Samples	X	n_X	d_X/pm	σ_X/pm^2
6a	N	4	212 ± 2	76 ± 32
	Cl^1	1	229 ± 5	100 ± 73
	Cl^2	1	267 ± 4	126 ± 85
	C	8	277 ± 4	465 ± 99
5a	N	4	204 ± 1	65 ± 10
	O	2	245 ± 2	
	C^1	7	288 ± 2	180 ± 29
6b	N	4	201.5 ± 0.7	53 ± 7
	O^1	1	229 ± 2	
	O^2	1	245 ± 3	
	C^1	5	285 ± 2	370 ± 180
	C^2	3	301 ± 3	
	S	2	351 ± 10	139 ± 42
5b	N	4	203 ± 1	77 ± 16
	O	2	239 ± 2	22 ± 15
	C^1	8	286 ± 2	71 ± 29

Noise level = 0.009, 0.012, 0.010, 0.016 for **6a**, **5a**, **6b**, and **5b**, respectively.

The best fit for each case is reported on Table 5. The carbon in α position of the nitrogen atoms of amino and pyridinyl groups was also included. For the molecular compounds the noise level was smaller allowing a more precise simulation with a larger number of fitted parameters. In particular, a third well defined FT peak arising at 322 pm (not shown here) accounts for farther carbons at about 350 pm (not reported) and sulfur at *ca* 360 pm (Table 5). These contributions are not seen clearly for materials **5a** and **5b** because of the higher noise level.

The closest copper neighbours N or O absorbers are simulated at 212, 204, 203 and 201.5 pm for **6a**, **5a**, **5b** and **6b**, respectively. Since O or N could not be distinguished, it stands for 4 N, 3N + 1O or 2N + 2O neighbours. These average distances are slightly higher than those of $[CuL_4^2](ClO_4)_2$ ($\langle d_{Cu\text{-}N}\rangle$ = 199 pm) where the coordination is 4N + 2O[50] and closer to those of $[Cu(L_4^2)Cl](ClO_4)$ where copper is pentacoordinated to 4N and 1 Cl ($\langle d_{Cu\text{-}N}\rangle$ = 205 pm).[51] Note that the perchlorate is a weak ligand located at 261 pm and not complexed, in the former and in the latter complexes, respectively. There is a defined trend on these distances that matches well with the trend noted for the g_1 component of the *g* tensor and the maximum of the absorption band in the visible region (see the discussion section).

The simulations confirm also the presence of elongated bonds in the first coordination sphere of copper. Both molecular compounds exhibit two Cu-X long distances of 229 and 267 pm (X = Cl) and, of 229 and 245 pm (X = O) for compounds **6a** (Cl) and **6b** (OTf), respectively. Note that the too short Cu–C distance of 277 pm in the molecular $Cu(L_4^2)Cl_2$, **6a**, is suspicious and denotes a simulation problem that may affect the simulation of the second type of chlorine neighbour at nearly the same distance (267 pm, Table 5). A multiple scattering EXAFS analysis would have been necessary, including farther neighbours. However, such study in the absence of a crystal structure is quite complicated and out of our scope here. Nonetheless, one can rely on reference compounds of known structure. A single Cl atom in a 4N + 1Cl environment, which lies at 242 pm in $[Cu(L_4^2)Cl](ClO_4)$ can be discarded.[51] The short Cu–Cl at 229 pm suggests that there is effectively a second Cl atom in the range 270–280 pm where copper lies in an octahedral 4N + Cl^1 + Cl^2 type of environment characterized by an asymmetric double μ-chloro bridge.[52] In addition, the average Cu–N distance ($\langle d_{Cu\text{–}N}\rangle$ = 212 pm) is rather large for **6a**, which indicates that one of the N atoms is in the elongation axis most likely at about 230 pm in such type of dimers. The same remark may also apply to the triflate salt **6b**, with two Cu–O distances (the simulation is at the limit in terms of quality since the QF is slightly above unity). These molecular complexes are currently being investigated further. Note that for the perchlorate $Cu(L_4^2)$ salt, XRD reveals a 4N + 2O environment with both Cu–O distances at 261 pm, *i.e.*, at an intermediate distance between those found in compound **6b**.[50,51,53]

For materials **5a** and **5b**, the situation seems less complicated since only one elongated distance for light atoms has been identified with no doubt. This is most likely two oxygen atoms at 245 and 239 pm, respectively. For material **5a**, which

had a slightly less noisy signal than that of material **5b**, a chlorine atom at 270 pm could also be simulated with a slight fit improvement (residue of ρ = 1.1% instead of 1.2%) but not sufficient to increase the fit quality (QF = 1.02 instead of 0.90). This makes the solution probable but not certain. For material **5b** such an eventuality could not be investigated safely because of the noise level. However, the position of the carbon atoms at 286 pm matches well the expected Cu–C distance for the carbons in α position from nitrogen atoms in the grafted Cu L_4^2 complexes and do not reveal any problem of simulation. Such single Cu–O elongated distance shorter than that found for the perchlorate counter ion[51,53] suggests the presence of a stronger ligand that could be either H_2O, Si–OH or $Si–O^-$ (*vide infra*).

Discussion

Distribution of the organic functions in the material

The molecular stencil technique applied here to prepare the internal surface of a 2D hexagonal mesostructured porous silica characterized by nanochannels of *ca.* 3.7 nm diameter (according to the BdB analysis) has already been discussed in a previous study.[17] Here, it is applied to separate bromopropyl tethers one to another using trimethylsilyl groups for further derivatisation by the polydentate pyridinylamino ligand L_4^2. Elemental analyses and quantitative IR studies lead to the conclusion that the surface is covered by trimethylsilyl (TMS), unreacted bromopropyl tethers (BPS), monotethered L_4^2 ligand (MTL_4^2) and ditethered L_4^2 ligand (DTL_4^2), as depicted in Scheme 2. These account for 0.18 TMS/Si, 0.008 BPS/Si, 0.012 MTL_4^2/Si and 0.009 DTL_4^2/Si, *i.e.*, 75, 3.3, 5 and 7.5% coverage, respectively (note that the ditethered L_4^2 accounts for two functions). An overall coverage of 91% is achieved. Reminding that the coverage is calculated in TMS equivalents, which is a smaller function than bromopropyl and L_4^2 moieties, one may reasonably assume that the surface is fully covered.

Note that the initial TMS coverage was 50% in material **2** before reaction with the bromopropyltrichlorosilane (Table 2). In material **3** the bromopropyl tethers cover only 16% of the surface, leading to an overall coverage of *ca* 70%. According to the site isolation effect, this situation is not optimal since 66% of TMS coverage would have been necessary before incorporation of the bromopropyl tether.[19] This may explain the presence of adjacent bromopropyl groups able to react with the same diamino ligand such as L_4^2. Such double S_N2 nucleophilic substitution on adjacent functions has already been illustrated and used to measure distances between adjacent bromopropyl functions in MCM-41 and SBA-15 silicas.[54] Anyhow, the combined effect of dilution by surface trimethylsilyl functions, incomplete reaction of the bromopropyl tethers and dual tethering on adjacent bromopropyl tethers creates a strong site separation on a rather hydrophobic surface.

Acido-basic properties of the surface

It is worth mentioning that a full TMS coverage does not mean a total disappearance of surface silanol groups. Indeed, a full TMS coverage (0.24 TMS/Si for 960 $m^2\ g^{-1}$) corresponds to 2.5 TMS nm^{-2}, approximately, while the silanol density of a non-silylated LUS silica is about 4.4 OH nm^{-2}.[55] This leaves about 1.9 silanol nm^{-2} unreacted on a non-calcined sample consistent with a strong and broad peak observed in the 3200–3600 cm^{-1} region in the IR spectrum (not shown here). The pK_a of the treated surface ranges from 7 to 10 with a distribution centred at about 9.[56] The grafted ligand L_4^2, has a pK_a of about 8.4 according to calculations.[57–59] Therefore, the protonation of the grafted ligands evidenced by XPS is not due to proton transfer from silanol as observed for aminopropyl groups (Fig. 4),[60,61] but rather to reaction with evolving HBr. The protonation level of 58% suggests a pH close to the highest pK_{a4} of L_4^2 ~8. Note that, the pK_{a1} and pK_{a2} of the pyridinyl moieties (~2) is lower than that of the amino group (pK_{a4} ~8). This clearly indicates that the protonation occurs on the latter exclusively.[59]

Metalation of the grafted protonated and unprotonated L_4^2

The metallation by mere contact with a copper salt ethanol solution clearly led to complexation of Cu(II) by the L_4^2 ligand according to diffuse reflectance spectra and the *g* tensors as characterized by EPR. According to the elemental analyses, the yield of complexation is at least 90% in both cases. The rotation blockage indicates also that these complexes are grafted to the support. But the question rises on the precise environment of the metal centre, given that 36% of the ligand seems to remain monoprotonated after metallation.

A closer analysis of the EPR parameters is proposed here to investigate the chelating properties of L_4^2 in the materials and in solution. Peisach and Blumberg have shown that A_z and g_z values are correlated to each other depending on the environment in the equatorial plane around copper.[62] Using a plot of A_z *vs.* g_z, they discriminate among the CuN_4, CuN_2O_2, CuO_4 types of coordination in natural enzymes. The same analysis has been applied here using an up-to-date Peisach and Blumberg type of diagram based on recent well defined coordination compounds similar to the copper complexes of this study.[63–73] The CuN_4 domains for A_z ~180–200 × 10^{-4} cm^{-1} and g_z ~2.19–2.25 can be ruled out. A more precise domain was obtained for $Cu(N_3O)$ type of coordination with ranges for A_z ~160–190 × 10^{-4} cm^{-1} and for g_z ~ 2.21–2.25. The latter matches better the present data for material **5a** and **5b** and compound **6b**. However, this type of analysis leads only to strong indications rather than certainties since the domains are not totally separated from another. Indeed, for $Cu(N_2O_2)$, the ranges are for A_z ~175–190 × 10^{-4} cm^{-1} and for g_z ~2.25–2.28. Both $(3N1O)_{xy}$ + O_z or $(2N2O)_{xy}$ + O_z environments give rise to similar *g* tensors of g_z = 2.25, g_y = 2.068 and g_x = 2.048 and $g_{||}$ = 2.25 and $g_\perp$ = 2.03, both with a water in apical position.[71] Another indication that the present *g* tensor matches better such a distorted environment with 2N or 3N instead of 4N is the low value of $g_\perp$ or g_x for the above cited species. This is even more obvious for a $(2N2O)_{xy}$ + O_z environment generated by bipyridine (bipy) or phenanthroline (phen), acetylacetonate (acac) and perchlorate reported by Su *et al.* with g_z = 2.249, g_y = 2.058 and g_x = 2.017 or g_z = 2.249, g_y = 2.059 and g_x = 2.020, respectively.[74]

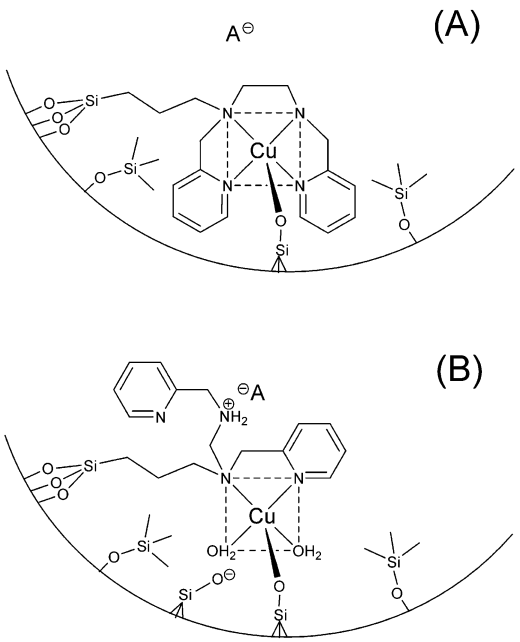

Fig. 7 Structural hypothesis on grafted copper complexes considering five instead of six neighbours for the sake of simplification: (A) 4 N atoms in equatorial position, 1 X atom in axial position, (B) 2 N and 2 O atoms (assuming here H_2O as ligands in both cases) in equatorial position, 1 X in axial position. In these structures X = SiO^-, other possibilities such as H_2O and SiOH O-donor ligands are not excluded.

Anyhow, it seems that a $(3N1O)_{xy}$ or even a $(2N2O)_{xy}$ environment around copper is more likely than the expected (4N) type for L_4^2 (Fig. 7). The rational is the partial protonation of the ligand in relation to the apparent pH of *ca* 10 of the solid before metallation. Indeed, this is unlikely to change after metallation and that may prevent all the N donor groups to bind the metal. This loss of coordination by a single protonated aminopyridinyl branch has been already observed in an Fe(III)L_5^3 complex where the L_5^3 turns from penta-coordinated to tricoordinated.[75] This has been also observed in a complex of copper(II) with the tripodal N_7 aminopyridinyl ligand (tpaa), which turns out to be pentadentate with one protonated aminopyridinyl branch not coordinated.[65] This is in favour with the $(2N2O)_{xy}$ environment. According to XPS, the resulting grafted $[Cu(L_4^2)]^{2+}$ and $[Cu(HL_4^2)]^{3+}$ relative concentrations should be about 64 and 36%, respectively. However, only one EPR signal is observed for both **5a** and **5b**. A dynamic equilibrium between both CuN_4 and CuN_2O_2 might be the answer, since it would generate an average signal consistent with an apparent intermediate CuN_3O environment. According to QM/MM MD calculations on $[Cu(H_2O)_6]^{2+}$, the first shell is statistically characterized by a 4 + 2 elongated octahedral coordination as expected. However, it undergoes a very fast scrambling of distances mixing the *x*, *y* and, *z* axes in the 10^{-13} s time scale whilst the ligand exchange is estimated in the 10^{-10} s time scale.[76] The experimental estimation of the Jahn–Teller axis inversion time using ^{17}O-NMR line broadening is not as fast as the theoretical estimation (~5.1 10^{-12} s).[77] However, it is still very short in comparison with the EPR time scale (~10^{-10} s). In addition, accelerated exchange processes have been experimentally shown with heteroligands (1 amino, 2 amino, bipy),[78] as corroborated by recent QM/MM MD calculations.[76b] In the present study, the ligand exchange with neighbouring water or silanol surface groups might probably stay too fast for EPR to be distinguishable. The absence of clear hyperfine structure due to ^{14}N nuclei usually clearly seen on the g_2 component is an indication of the dynamic nature of the EPR species. EPR measurements down to 100 K (limit of our cryostat) does not increase the resolution indicating a tendency of EPR signal broadening consistent with the dynamic characteristics of the EPR active species. Further investigation at lower temperature is in progress.

The EXAFS study reveals that the coordination can be described with rather six neighbours than five though limited accuracy due to the complexity of the copper environment leaves some margin in between both cases. Furthermore, N or O atoms are not distinguishable by this technique. Therefore, only distances are exploited with a focus on consistency with the data obtained from the other techniques.

The average distance obtained for the closest neighbours, *i.e.* O or N atoms in the basal (or equatorial) plan, decreases from 212 to 201 pm for **6a**, **5a**, **5b** and **6b**, in this order while the absorption band in the visible region shifts from 786 down to 578 nm, respectively. Moreover, g_1 roughly decreases along the same sequence. This is consistent with an increase of the crystal field along this series, indeed, the shorter the distances the stronger the ligand field (LF). Effectively, the shorter wavelength of the absorption band in the visible region is consistent with the increased energy splitting of the d orbitals in the LF. Despite some obvious distortion, a D_{4h} symmetry is a reasonable first order approximation of such hexa-coordinated copper complexes[79] where the main contribution to this band is the $B_{2g} \leftarrow B_{1g}$ electronic transition.[74,80] This transition is directly related to ΔE_{xy}, the energy difference between the metal orbitals $d_{x^2-y^2}$ (ground state in D_{4h} d^9 Cu^{2+} ion) and d_{xy}, and, therefore, to the LF strength in the *xy* plane. In addition, (g_1 − 2.023) is inversely proportional to ΔE_{xy}, which explains its decrease along the series.[81]

According to molecular compounds **6a** and **6b**, one of the driving forces for the LF increase in the *xy* plane, is the ligand exchange by triflate for chloride in the apical axis.[50,51,63,82] Accordingly, the increase from **6a** to **5a** is consistent with a partial removal of chloride for a weaker ligand. EXAFS shows that the nearest apical neighbours are indeed oxygen atoms at 245 ± 3 pm. For **5b**, the apical atom is also an oxygen but at a slightly closer distance of 239 ± 2 pm that is too short to be a triflate ion. Despite the convergence of environment for both grafted complexes issued from the chloride or the triflate salt, some differences still remain that strongly suggest the presence of the remaining counter ions in the vicinity of copper more likely in the second coordination sphere.

Another driving force for the LF evolution is the partial protonation of L_4^2 decreasing the chelation from four to two, and resulting in a fraction of copper involved in a $(2N2O)_{xy}$ + O_z type of environment. Examples in the literature show that this type of environment are rather penta-coordinated and obtained from bipyridine (bipy) or phenanthroline (phen) types of ligand: $(3N1O)_{xy}$ + O_z[66] and $(2N2O)_{xy}$ + O_z[67,68,71] They are also the only cases that explain the low g_x values

found in the present study (Table 4). It is worth noting that in crystallized molecular analogues, the apical water molecules are expected at *ca.* 219 pm,[66] 226 pm[71] or even at 229.2 pm.[83] These distances are shorter than those found here for **5a** and **5b** where the metal environment is quite different including the presence of weaker ligands as surface silanol or silanolate (Fig. 7).

The rationale here is the coexistence of octahedral $Cu(N_4)_{xy}(O_2)_z$ with rather elongated Cu–O_z distances in equilibrium with a square planar pyramidal $Cu(N_2O_2)_{xy}(O)_z$ species with neutral and monoprotonated grafted L_4^2 ligand. The unique EPR signal suggests a rapid equilibrium exchange between both structures. This last point needs to be further investigated.

Conclusions

A bio-inspired design of materials containing grafted L_4^2 copper(II) complexes has been achieved according to the five-step retrosynthetic route of Fig. 2. It appears that (i) the substitution conditions that were chosen to avoid function degrafting lead to *ca* 80% of bromine displacement, (ii) the removal of side products such as HCl or HBr is incomplete in the presence of amino groups, that stay partially monoprotonated (~58%) in the confined space of the nanochannels, (iii) the ligand grafting occurs *via* two modes, *i.e.*, mono (40%) and dual (60%) tethering and, (iv) the metallation yield of the ligand is better than 90%. The partial retention of proton after the metallation by copper(II) introduces some uncertainties in the chelating properties of the L_4^2 ligand, which is likely acting both as a monoprotonated bidentate ligand and as a neutral tetradentate ligand. Washing the material with a base such as triethylamine would likely deprotonate the ligand and favour the tetradentate chelation to copper ion (work in progress). Indeed, in natural proteins, only low pK_a N-donor ligands such as imidazole (p$K_a \sim 7$) complex metal ions while amino groups are always protonated (p$K_a > 10$) and, therefore, not complexing. The bio-inspired type of design proposed here can be applied to many different ligands and metals opening a wide range of possibilities to develop new types of heterogeneous catalysts with high molecular definition as shown here.

Acknowledgements

The authors thank the French program "Energie, Conception Durable 2004" (ACI ECD009 BioCatOx) for financial support. The authors are also grateful to the SpLine/Spanish CRG beamline (BM25) at European Synchrotron Radiation Facility (ESRF) in Grenoble, France, and especially to Germán Castro for his useful help in XAS measurements.

References

1 S. J. Lippard and J. M. Berg, *Principles of Bioinorganic Chemistry*, University Science Books, Mill Valley, CA, 1994.
2 J. L. Pierre, *Chem. Soc. Rev.*, 2000, **29**, 251.
3 (*a*) S. Itoh, M. Taki, P. Holland, W. B. Tolman and L. Que, *J. Inorg. Biochem.*, 1999, **74**, 33; (*b*) L. M. Mirica, X. Ottenwaelder and T. D. P. Stack, *Chem. Rev.*, 2004, **104**, 1013; (*c*) A. Decker and E. I. Solomon, *Curr. Opin. Chem. Biol.*, 2005, **9**, 152.
4 M. K. Zart, T. N. Sorrell, D. Powell and A. S. Borovik, *Dalton Trans.*, 2003, 1986.
5 S. Xiang, Y. L. Zhang, Q. Xin and C. Li, *Angew. Chem., Int. Ed.*, 2002, **41**, 821.
6 D. Rechavi, B. Albela, L. Bonneviot and M. Lemaire, *Tetrahedron*, 2005, **61**, 6976.
7 J. J. Girerd, F. Banse and A. J. Simaan, *Struct. Bonding*, 2000, **97**, 145.
8 M. Costas, M. P. Mehn, M. P. Jensen and L. Que, *Chem. Rev.*, 2004, **104**, 939.
9 K. Chen and L. Que, *Chem. Commun.*, 1999, 1375.
10 V. Balland, D. Mathieu, Y. M. N. Pons, J. F. Bartoli, F. Banse, P. Battioni, J. J. Girerd and D. Mansuy, *J. Mol. Catal. A*, 2004, **215**, 81.
11 N. Raffard, F. Banse, K. Miki, M. Nierlich and J.-J. Girerd, *Eur. J. Inorg. Chem.*, 2002, 1941.
12 M. C. Linder, *Biochemistry of Copper*, Plenum Press, NY, 1991, pp. 1–13.
13 C. Adreini, L. Banci, I. Bertini and A. Rosato, *J. Proteome Res.*, 2007, **7**, 209.
14 P. Gamez, P. G. Aubel, W. L. Driessen and J. Reedijk, *Chem. Soc. Rev.*, 2001, **30**, 376.
15 J. S. Beck, J. C. Vartuli, W. J. Roth, M. E. Leonowicz, C. T. Kresge, K. D. Schmitt, C. T. W. Chu, D. H. Olson, E. W. Sheppard, S. B. McCullen, J. B. Higgins and J. L. Schlenker, *J. Am. Chem. Soc.*, 1992, **114**, 10834.
16 (*a*) D. Y. Zhao, J. L. Feng, Q. S. Huo, N. Melosh, G. H. Fredrickson, B. F. Chmelka and G. D. Stucky, *Science*, 1998, **279**, 548; (*b*) D. Y. Zhao, Q. S. Huo, J. L. Feng, B. F. Chmelka and G. D. Stucky, *J. Am. Chem. Soc.*, 1998, **120**, 6024.
17 S. Calmettes, B. Albela, O. Hamelin, S. Ménage, F. Miomandre and L. Bonneviot, *New J. Chem.*, 2008, **32**, 727.
18 C. H. Lee, S. T. Wong, T. S. Lin and C. Y. Mou, *J. Phys. Chem. B*, 2005, **109**, 775.
19 S. Abry, B. Albela and L. Bonneviot, *C. R. Chim.*, 2005, **8**, 741.
20 S. Abry, PhD Thesis, Ecole Normale Supérieure de Lyon, Université de Lyon, Lyon, France, 2007.
21 H. A. Goodwin and F. Lions, *J. Am. Chem. Soc.*, 1960, **82**, 5013.
22 L. Bonneviot, M. Morin and A. Badiei, *World Pat.*, WO 01/55 031A1, 2001.
23 P. Reinert, B. Garcia, C. Morin, A. Badiei, P. Perriat, O. Tillement and L. Bonneviot, in *Nanotechnology in Mesostructured Materials*, Elsevier Science, Amsterdam, 2003, p. 133.
24 (*a*) A. Michalowicz, *Logiciels Pour la Chimie*, Societé Française de Chimie, Paris, 1991, p. 102; (*b*) A. Michalowicz, *J. Phys. IV*, 1997, **7**, 235–236.
25 (*a*) B. K. Teo, *Inorganic Chemistry Concepts, EXAFS: Basic Principles and Data Analysis*, Springer-Verlag, Berlin, 1986; (*b*) D. C. Königsberger, *X-ray Absorption Principles, Applications, Techniques of EXAFS, SEXAFS and XANES*, Wiley, New York, 1988, vol. 9; (*c*) F. W. Lytle, D. E. Sayers and E. A. Stern, *Physica B* 1989, **158**, 710: information on error analysis procedures used in this program is available at http://scon155.phys.msu.su/~IXS/survey/errors/, it follows the recommendation of the Standards and criteria subcommittee of the International XAFS Society (IXS) (http://www.i-x-s.org/).
26 W. H. MacMaster, N. Kerr Del Grande, J. H. Nallet and J. H. Hubbel, *Compilation of X-ray Cross Sections*, National Technical Information Services, Springfield, VA, 1969.
27 J. P. Fitts, P. Persson, G. E. Brown, Jr and G. A. Parks, *J. Colloid Interface Sci.*, 1999, **220**, 133: for alumina supported Cu(II) glutamate, the first multiple scattering pathway arises betweem 300 pm and 400 pm.
28 F. Carrera, E. Sanchez-Marcos, P. J. Merkling, J. Chaboy and A. Munoz-Paez, *Inorg. Chem.*, 2004, **43**, 6674: in both $[Cu(en)_2]^{2+}$, $[Cu(NH)_4]^{2+}$ complexes, the multi-scattering is found negligible above 2.9 Å.
29 (*a*) J. J. Rehr, S. I. Zablinsky and R. C. Abers, *Phys. Rev. Lett.*, 1992, **69**, 3397; (*b*) J. J. Rehr, *Jpn. J. Appl. Phys.*, 1993, **32**, 8; (*c*) J. J. Rehr, J. Mustre de Leon, S. I. Zablinsky and R. C. Albers, *J. Am. Chem. Soc.*, 1991, **113**, 5135; (*d*) J. Mustre de Leon, J. J. Rehr, S. I. Zablinsky and R. C. Albers, *Phys. Rev. B*, 1991, **44**, 4146; (*e*) J. J. Rehr and R. C. Albers, *Phys. Rev. B*, 1990, **41**, 8139.

30 G. Vlaic, D. Andreatta, A. Cepparo, P. E. Colavita, E. Fonda and A. Michalowicz, *J. Synchrotron Radiat*., 1999, **6**, 225.
31 A. Badiei, L. Bonneviot, N. Crowther and G. M. Ziarani, *J. Organomet. Chem*., 2006, **691**, 5911.
32 (*a*) M. H. Lim and A. Stein, *Chem. Mater*., 1999, **11**, 3285; (*b*) T. Yokoi, H. Yoshitake and T. Tatsumi, *J. Mater. Chem*., 2004, **14**, 951.
33 M. W. McKittrick and C. W. Jones, *Chem. Mater*., 2003, **15**, 1132.
34 (*a*) O. Clause, L. Bonneviot, M. Che and H. Dexpert, *J. Catal*., 1991, **130**, 21; (*b*) O. Clause, M. Kermarec, L. Bonneviot, F. Villain and M. Che, *J. Am. Chem. Soc*., 1992, **114**, 4709.
35 K. S. W. Sing, D. H. Everett, R. A. W. Haul, L. Moscou, R. A. Pierotti, J. Rouquerol and T. Siemieniewska, *Pure Appl. Chem*., 1985, **57**, 603.
36 J. S. Beck, J. C. Vartuli, W. J. Roth, M. E. Leonowicz, C. T. Kresge, K. D. Schmitt, C. T. W. Chu, D. H. Olson, E. W. Sheppard, S. B. McCullen, J. B. Higgins and J. L. Schlenker, *J. Am. Chem. Soc*., 1992, **114**, 10834.
37 C. T. Kresge, J. C. Vartuli, W. J. Roth and M. E. Leonowicz, in *Mesoporous Crystals and Related Nano-Structured Materials*, Wiley, NJ, 2004, pp. 53–72.
38 C. T. Kresge, J. C. Vartuli, W. J. Roth, M. E. Leonowicz, J. S. Beck, K. D. Schmitt, C. T. W. Chu, D. H. Olson, E. W. Sheppard, S. B. McCullen, J. B. Higgins and J. L. Schlenker, in *Science and Technology in Catalysis 1994*, 1995, pp. 11–19.
39 S. Calmettes, PhD Thesis, Ecole Normale Supérieure de Lyon, Université de Lyon, Lyon, France, 2008.
40 *Handbook of X-ray Photoelectron Spectroscopy*, ed. J. Chastain, Perkin-Elmer Corp., Physical Electronics Division, Eden Prairie, MN, 1992.
41 J. Garcia-Martin, R. Lopez-Garzon, M. L. Godino-Salido, R. Cuesta-Martos, M. D. Gutierrez-Valero, P. Arranz-Mascaros and H. Stoeckli-Evans, *Eur. J. Inorg. Chem*., 2005, 3093.
42 (*a*) O. Clause, L. Bonneviot, M. Che, M. Verdaguer, F. Villain, D. Bazin and H. Dexpert, *J. Chim. Phys. Phys. Chim. Biol*., 1989, **86**, 1767; (*b*) L. Bonneviot, O. Legendre, M. Kermarec, D. Olivier and M. Che, *J. Colloid Interface Sci*., 1990, **134**, 534: previous studies on nickel(II) ammine complexes adsorbed on silica show that SiO– is a weaker ligand than H_2O, leading to a weaker ligand field.
43 (*a*) L. Trouillet, T. Toupance, F. Villain and C. Louis, *Phys. Chem. Chem. Phys*., 2000, **2**, 2005; (*b*) G. W. Smith and H. W. Jacobson, *J. Phys. Chem*., 1956, **60**, 1008.
44 G. Martini and L. Burlamacchi, *J. Phys. Chem*., 1979, **83**, 2505.
45 G. Martini and V. Bassetti, *J. Phys. Chem*., 1979, **83**, 2511.
46 A. H. Maki, A. Davison, N. Edelstein and R. H. Holm, *J. Am. Chem. Soc*., 1964, **86**, 4580.
47 M. J. Bew, B. J. Hathaway and R. J. Fereday, *J. Chem. Soc., Dalton Trans*., 1972, 1229.
48 (*a*) D. E. Billing, R. J. Dudley, B. J. Hathaway and A. Tomlinso, *J. Chem. Soc. A: Inorg. Phys. Theor*, 1971, 691; (*b*) M. J. Bew, R. J. Dudley, R. J. Fereday, R. C. Slade and B. J. Hathaway, *J. Chem. Soc. A: Inorg. Phys. Theor*., 1971, 1437.
49 F. Beland, A. R. Badiei, M. Ronning, D. Nicholson and L. Bonneviot, *Phys. Chem. Chem. Phys*., 1999, **1**, 605.
50 E. V. Rybak-Akimova, A. Y. Nazarenko, L. Chen, P. W. Krieger, A. M. Herrera, V. V. Tarasov and P. D. Robinson, *Inorg. Chim. Acta*, 2001, **324**, 1.
51 Crystal structure code KOQFEB, Cambridge data base.
52 J. Manzur, A. Vega, A. M. Garcia, C. Acuna, M. Sieger, B. Sarkar, M. Niemeyer, F. Lissnerll, T. Schleid and W. Kaim, *Eur. J. Inorg. Chem*., 2007, 5500: tridentate pyridinylamino ligand (pyridin-2-ylethyl)(pyridin-2-ylmethyl)benzamine), $3N + Cl^1 + Cl^2$ environment with asymmetric double Cu–Cl^2–Cu, $d_{Cu–Cl}$ = 229.8 and 279.1 pm.
53 P. V. Bernhardt, *J. Am. Chem. Soc*., 1999, **119**, 771.
54 T. Miyajima, S. Abry, W. J. Zhou, B. Albela, L. Bonneviot, Y. Oumi, T. Sano and H. Yoshitake, *J. Mater. Chem*., 2007, **17**, 3901.
55 R. F. de Farias and C. Airoldi, *J. Therm. Anal. Calorim*., 1998, **53**, 751: silanol density calculated from mass loss between 150–1000 °C using TGA (5% weight loss for a residual mass of 82.8%).
56 R. K. Iler, *Chemistry of Silica: Solubility Polymerization Colloid and Surface Properties and Biochemistry*, Wiley-Interscience, New York, 1979.
57 H. Lu, X. Chen and C. G. Zhan, *J. Phys. Chem. B*, 2007, **111**, 10599.
58 H. A. Carlson, J. M. Briggs and J. A. McCammon, *J. Med. Chem*., 1999, **42**, 109.
59 http://intro.bio.umb.edu/111-112/OLLM/111F98/newclogp.html. Since the present material contains confined water in a relatively hydrophobic media the calculation of pH and pK_a have to be taken with caution. Nonetheless, one may consider the pyridinyl-amino function as an internal pH probe. The theoretical predictions of pK_{a1}, pK_{a2}, pK_{a3}, pK_{a4} are 1.9, 2.5, 5.2, and 8.0, respectively. Note that this software calculates correctly pK_a of primary, secondary and tertiary amines in water, 10, 10.5 and 9.6, respectively, and for pyridine (5,1) and a pyridin-2-ylmethamine (2.6 and 8.6).
60 M. Etienne and A. Walcarius, *Talanta*, 2003, **59**, 1173.
61 (*a*) B. V. Zhmud and A. B. Pechenyi, *J. Colloid Interface Sci*., 1995, **173**, 71; (*b*) A. A. Golub, A. I. Zubenko and B. V. Zhmud, *J. Colloid Interface Sci*., 1996, **179**, 482.
62 J. Peisach and W. E. Blumberg, *Arch. Biochem. Biophys*., 1974, **165**, 691.
63 (*a*) J. R. Hartman, R. W. Vachet, W. Pearson, R. J. Wheat and J. H. Callahan, *Inorg. Chim. Acta*, 2003, **343**, 119; (*b*) J. A. R. Hartman, A. L. Kammier, R. J. Spracklin, W. H. Pearson, M. Y. Combariza and R. W. Vachet, *Inorg. Chim. Acta*, 2004, **357**, 1141.
64 H. Abe and J. Shimada, *J. Phys. Soc. Jpn*., 1957, **12**, 1255.
65 C. Gérard, A. Mohamadou, J. Marrot, S. Brandes and A. Tabard, *Helv. Chim. Acta*, 2005, **88**, 2397.
66 F. Belanger-Gariepy, R. Faure, F. Hueso-Urena, M. N. Moreno-Carretero, J. A. Rodriguez-Navarro and J. M. Salas-Peregrin, *Polyhedron*, 1998, **17**, 1747.
67 C. Fernandes, G. L. Parrilha, J. A. Lessa, L. J. M. Santiago, M. M. Kanashiro, F. S. Boniolo, A. J. Bortoluzzi, N. V. Vugman, M. H. Herbst and A. Horn, *Inorg. Chim. Acta*, 2006, **359**, 3167.
68 O. O. E. Onawumi, O. O. P. Faboya, O. A. Odunola, T. K. Prasad and M. V. Rajasekharan, *Polyhedron*, 2008, **27**, 113.
69 P. Deschamps, N. Zerrouk, I. Nicolis, T. Martens, E. Curis, M. F. Charlot, J. J. Girerd, T. Prange, S. Benazeth, J. C. Chaumeil and A. Tomas, *Inorg. Chim. Acta*, 2003, **353**, 22.
70 H. J. Scholl and J. Huttermann, *J. Phys. Chem*., 1992, **96**, 9684.
71 A. Tovar-Tovar, L. Ruiz-Ramirez, A. Campero, A. Romerosa, R. Moreno-Esparza and M. J. Rosales-Hoz, *J. Inorg. Biochem*., 2004, **98**, 1045.
72 D. Dobrzynska, M. Duczmal, J. Jezierska and L. B. Jerzykiewicz, *Polyhedron*, 2002, **21**, 2381.
73 G. Izzet, Y. M. Frapart, T. Prange, K. Provost, A. Michalowicz and O. Reinaud, *Inorg. Chem*., 2005, **44**, 9743.
74 C. C. Su, S. P. Wu, C. Y. Wu and T. Y. Chang, *Polyhedron*, 1995, **14**, 267.
75 V. Balland, F. Banse, E. Anxolabéhère-Mallart, M. Ghiladi, T. A. Mattioli, C. Philouze, G. Blondin and J.-J. Girerd, *Inorg. Chem*., 2003, **42**, 2470; L_5^3 is a pentadentate aminopyridine ligand of the same family as L_4^2.
76 (*a*) C. F. Schwenk and B. M. Rode, *ChemPhysChem*, 2003, **4**, 931; (*b*) C. F. Schwenk and B. M. Rode, *Phys. Chem. Chem. Phys*., 2003, **5**, 3418.
77 D. H. Powell, L. Helm and A. E. Merbach, *J. Chem. Phys*., 1991, **95**, 9258.
78 (*a*) I. Nagypal and F. Debreczeni, *Inorg. Chim. Acta*, 1984, **81**, 69; (*b*) F. Debreczeni and I. Nagypal, *Inorg. Chim. Acta*, 1982, **57**, 135; (*c*) I. Fabian, *Inorg. Chem*., 1993, **32**, 1184.
79 M. Atanasov, P. Comba, B. Martin, V. Muller, G. Rajaraman, H. Rohwer and S. Wunderlich, *J. Comput. Chem*., 2006, **27**, 1263.
80 (*a*) B. J. Hathaway and D. E. Billing, *Coord. Chem. Rev*., 1970, **5**, 143; (*b*) B. Murphy and B. Hathaway, *Coord. Chem. Rev*., 2003, **243**, 237.
81 D. Kivelson and R. Neiman, *J. Chem. Phys*., 1961, **35**, 149.
82 It is known that Cl^- is a stronger ligand than triflate, therefore a stronger ligand in the *z* axis will decrease the LF in the *xy* plane consistently with many examples including in such type of complexes.
83 N. A. Bailey, D. E. Fenton, M. V. Franklin and M. Hall, *J. Chem. Soc., Dalton Trans*., 1980, 984.

